

# Comparison of Dynamic Characteristics Between Virtual Synchronous Generator and Droop Control in Inverter-Based Distributed Generators

Jia Liu, *Student Member, IEEE*, Yushi Miura, *Member, IEEE*, and Toshifumi Ise, *Member, IEEE*

**Abstract**—In recent researches on inverter-based distributed generators, disadvantages of traditional grid-connected current control, such as no grid-forming ability and lack of inertia, have been pointed out. As a result, novel control methods like droop control and virtual synchronous generator (VSG) have been proposed. In both methods, droop characteristics are used to control active and reactive power, and the only difference between them is that VSG has virtual inertia with the emulation of swing equation, whereas droop control has no inertia. In this paper, dynamic characteristics of both control methods are studied, in both stand-alone mode and synchronous-generator-connected mode, to understand the differences caused by swing equation. Small-signal models are built to compare transient responses of frequency during a small loading transition, and state-space models are built to analyze oscillation of output active power. Effects of delays in both controls are also studied, and an inertial droop control method is proposed based on the comparison. The results are verified by simulations and experiments. It is suggested that VSG control and proposed inertial droop control inherits the advantages of droop control, and in addition, provides inertia support for the system.

**Index Terms**—DC-AC power converters, distributed power generation, droop control, microgrids, power control, power system dynamics, power system modeling, renewable energy sources (RES), state-space methods, virtual synchronous generator (VSG).

## I. INTRODUCTION

**T**O solve environmental issues and energy crisis, distributed generators (DGs) using renewable energy sources (RES), such as photovoltaics and wind turbines, have been developed in recent decades. These types of DGs are usually composed of a dc link and two stages: input-side converter and grid-side converter. Although the input-side converter and its controller differ according to energy sources and technologies, the grid-side converter, which is usually a dc/ac inverter, can be controlled in the same way [1].

A traditional control method for an inverter-based DG is grid-connected current control. In this control method, commonly a phase-locked loop is used to synchronize the inverter to the grid and the output current is controlled to transfer predefined active

and/or reactive power to the grid. Two major drawbacks of this control method have been pointed out. First, DGs equipped with this control do not have grid-forming ability; therefore, they are not able to work in stand-alone mode. Secondly, their penetration rate is limited because they have no inertia, which retards the growth of RES penetration. To make DGs have grid-forming and power-sharing ability, droop control, a control method for real and reactive power regulation by imitating the parallel operation characteristics of synchronous generators (SGs), was originally proposed in [2] for uninterruptible power supply (UPS) systems, and has been developed into a general approach for parallel inverters [3], especially in microgrids [4]–[30] and UPS systems [31], [32].

There are several variants of droop control. To be applied in low voltage (LV) network, in which the line impedance is resistive,  $P$ - $V$  droop control [5]–[8], instead of traditional  $P$ - $\omega$  droop [2]–[4], has been proposed to improve power sharing and stability. Moreover, a virtual frequency-voltage frame method is proposed to solve this problem in any giving condition of line impedance  $R/X$  ratio [9]. In the other hand,  $P$ - $\omega$  droop can still be applied in LV network by adding virtual output impedance to make the total line impedance inductive [11]–[13], [31], [32]. In microgrid applications, droop control usually plays the role of primary control in a hierarchic structure, in which secondary control is designed to keep the frequency and voltage around the nominal value [10]–[15], and/or to obtain accurate reactive power [14]–[19], harmonic and unbalance power sharing [17] and voltage harmonic compensation [15], [20] in islanded mode, and tertiary control is designed to manage synchronization to the main grid, power-flow control in grid-connected mode and optimal operation [12]–[13]. As secondary and tertiary control need communication command from a central controller, issues are still encouraged to be solved with a wireless manner, such as it is proposed in [20]–[25] for accurate power sharing, in [26] for operation with unbalance load and nonlinear load, in [27] for harmonic components dispatch, and in [28] for reducing frequency and voltage deviation. It has also been demonstrated that optimization of droop coefficient [29] and supplementary droop control loop [30] can help to enhance system stability.

However, DGs equipped with droop control still have no inertia support for the power system. Therefore, a new control method, called virtual synchronous generator (VSG) [33]–[42], or virtual synchronous machine [43], or synchronverter [44], [45], has been proposed to mimic not only the steady-state characteristics of SGs, but also their transient characteristics by applying swing equation to enhance the inertia. To facilitate

Manuscript received April 10, 2015; revised June 16, 2015; accepted August 2, 2015. Date of publication August 7, 2015; date of current version December 10, 2015. This paper was presented in part at the *International Power Electronics Conference*, Hiroshima, Japan, in May 2014. Recommended for publication by Associate Editor J. M. Guerrero.

The authors are with the Division of Electrical, Electronic and Information Engineering, Osaka University, Osaka 565-0871, Japan (e-mail: liu@pe.eei.eng.osaka-u.ac.jp; miura@eei.eng.osaka-u.ac.jp; ise@eei.eng.osaka-u.ac.jp).

Color versions of one or more of the figures in this paper are available online at <http://ieeexplore.ieee.org>.

Digital Object Identifier 10.1109/TPEL.2015.2465852

the explication, all methods with the idea of virtual inertia are called VSG control in this paper. With proper energy management, DGs equipped with VSG control can use their dc-link energy storage to play the role of the kinetic energy reservoir in the rotating mass of SGs, and therefore, provide virtual inertia to the system. In earlier researches on VSG control, control methods are designed for energy storages rather than DGs [34]–[36], [46], [47], to make the energy storages behave as dedicated frequency compensators. Recent years, various approaches of VSG control for DGs have been developed [37], [38], [43]–[45]. In these approaches, it is usually necessary to calculate complete SG models, which makes the algorithm complicated and therefore requires higher processor capacity. In a simpler method, proposed in [39]–[42], only the essential element of VSG, i.e., the swing equation, is considered, and the rotor frequency is calculated directly by solving swing equation using the iterative method. Oscillation damping method [41] and alternating moment of inertia [42] are proposed to improve transient response and avoid overcurrent. Moreover, it is reported that modification of droop coefficient in droop control can also contribute to total inertia of the system [48]. Besides providing inertia, VSG control can be used to improve transient power sharing between SG and DG in a microgrid [49].

Comparison between droop control and VSG control in a VSC-HVDC transmission system is demonstrated in [50], to show that the virtual inertia helps to reduce maximum frequency excursion during a short-time fault, and during loading transition when secondary frequency control is applied; however, detailed theoretical analysis is not provided. A comparison on transient active power performance is presented in [51], but the difference on inertia and transient frequency is not discussed in this paper. A theoretical comparison on frequency and inertia is discussed in [52]; however, oscillation phenomenon of VSG control is not studied and several points need to be further developed.

In this paper, dynamic characteristics of VSG control and droop control are compared to understand the difference of the two control methods caused by the presence of swing equation. Small-signal models of both methods are built, for both stand-alone mode and SG-connected mode, to calculate theoretical step responses of frequency change, in order to understand the inertia effect caused by the virtual inertia. Effects of delays in governor and  $P$  droop controller are also evaluated, and an approximated VSG control based on droop control, i.e., inertial droop control, is proposed. Although the idea of using first-order lag unit in droop control to emulate virtual inertia is already mentioned in [50] and [51], it is further developed in this paper by adding first-order lag unit to emulate the damping factor. State-space models of both methods are constructed to study oscillation of output active power. Theoretical results are verified by simulations using PSCAD/EMTDC and by experiments of a scale-down system.

It should be pointed out that although the VSG control scheme studied in this paper is proposed in [39]–[42], the results should also be valid for other VSG control schemes with similar small-signal models. Moreover, the small-signal models and state-space models presented in this paper provide a general method

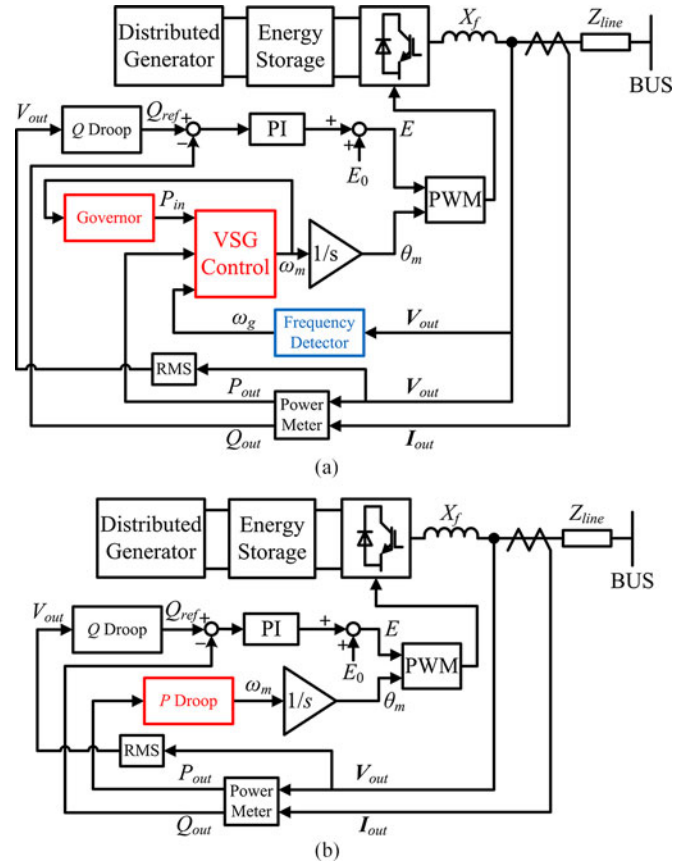


Fig. 1. Basic control systems of (a) VSG and (b) droop control.

for analyses of dynamic performances of VSG and droop control, which should be helpful tools for future studies on this topic.

## II. PRINCIPLE OF VSG AND DROOP CONTROL

Fig. 1 shows the basic control system of VSG control proposed in [39]–[42] and that of analogous droop control. The reactive power control is identical in both control methods. Therefore, in this paper, only the differences of active power control are studied.

The swing equation in the block “VSG Control” of VSG in Fig. 1(a) can be written as

$$P_{in} - P_{out} = J\omega_m \frac{d\omega_m}{dt} + D^* S_{base} \frac{\omega_m - \omega_g}{\omega_0} \quad (1)$$

where  $P_{in}$  is the virtual shaft power determined by the governor,  $P_{out}$  is the measured output power,  $S_{base}$  is the power rating of DG,  $J$  is the virtual inertia,  $D$  is the virtual damping factor, superscript \* indicates per unit value,  $\omega_m$  is the virtual rotor angular frequency,  $\omega_g$  is the angular frequency of the point where the voltage sensor is installed, and  $\omega_0$  is the nominal angular frequency. In this paper, it is assumed that the number of pairs of poles of VSG is 1.

The block ‘‘Governor’’ in Fig. 1(a) is a  $\omega$ - $P$  droop controller which can be represented as

$$P_{in} = P_0 - k_p^* S_{base} \frac{\omega_m - \omega_0}{\omega_0} \quad (2)$$

where  $P_0$  is the set value of active power, and  $k_p^*$  is the droop coefficient (in per unit)

Let  $k_p = (k_p^* S_{base})/\omega_0$ ,  $D = (D^* S_{base})/\omega_0$ , and eliminate  $P_{in}$  from (1) and (2), so that

$$P_0 - k_p (\omega_m - \omega_0) - P_{out} = J\omega_m \frac{d\omega_m}{dt} + D (\omega_m - \omega_g). \quad (3)$$

In [50] and [51],  $\omega_g$ , which is a measured parameter in this paper to provide the synchronous frequency for damping power calculation, is replaced by a constant value, i.e., nominal frequency  $\omega_0$ ; thus, the damping factor  $D$  becomes equivalent to droop coefficient  $k_p$ . This modification of swing equation results in a simpler model, and as a result, the dedicated governor can even be omitted, as it is presented in [51]. In this case, however, no damping effect caused by damper winding is emulated, which may result in larger output power oscillation.

The relation in ‘‘ $P$  Droop’’ of droop control in Fig. 1(b) is

$$\omega_m = -\frac{P_{out} - P_0}{k_p} + \omega_0. \quad (4)$$

Let  $J = 0$ ,  $D = 0$ , (3) is equivalent to (4). In other words, droop control can be considered as a particular case of VSG control, where both inertia and damping factor are set to zero.

### III. COMPARISONS OF TRANSIENT RESPONSES OF FREQUENCY

In this section, first, small-signal models of VSG and droop control are built for both stand-alone mode and SG-connected mode. Then, based on these models, step responses of frequency change during a loading transition are calculated and then compared to corresponding simulation results. The system with slower change of frequency is preferable, because lower  $df/dt$  indicates larger inertia. System with smaller inertia is prone to exceed the  $df/dt$  threshold of relays during a large loading transition, which may lead to unnecessary tripping and load shedding. Moreover, system with larger inertia suffers smaller maximum frequency excursion during a short time fault, and during a loading transition when secondary control is applied, as it is demonstrated in [50].

To simplify the model in order to focus on active power control, reactive power control of both control methods is inactivated in this study. Therefore, in Fig. 1,  $E$  is fixed to  $E_0$ .

#### A. Stand-alone Mode

First of all, a stand-alone system shown in Fig. 2(a) is studied. The cable between DG and load is considered inductive, and its resistance can be neglected. It is always the case in high voltage (HV) network, and even in LV network, it becomes true when an inductive virtual output impedance is applied [11]–[13], [31], [32]. By calculating power flow, (5) can be deduced

$$\Delta P_{out\_dg} = E_{dg} V_{bus} \cos \delta_{dg} \Delta \delta_{dg} / X_{dg} \quad (5)$$

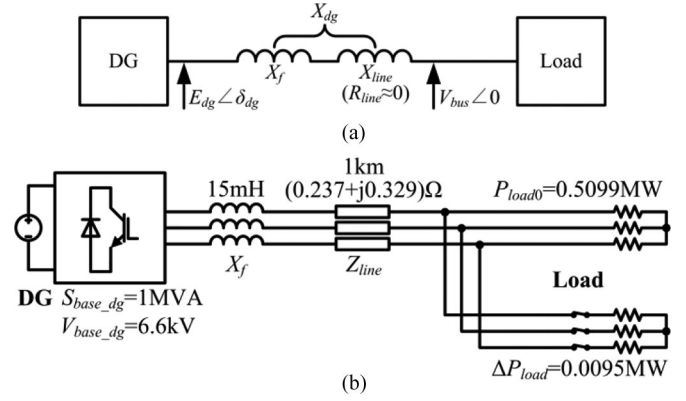


Fig. 2. (a) Stand-alone mode model. (b) Simulation circuit of stand-alone mode.

where subscript ‘‘ $dg$ ’’ indicates parameters related to DG, and  $X_{dg} = X_f + X_{line}$  is the total output reactance of DG.

Knowing that  $\Delta \delta_{dg} = (\Delta \omega_{m\_dg} - \Delta \omega_{bus}) / s$ , where  $\omega_{bus}$  is bus frequency, let  $K_{dg} = (E_{dg} V_{bus} \cos \delta_{dg}) / X_{dg}$  which is the synchronizing power coefficient of DG, so that (5) becomes

$$s \Delta P_{out\_dg} \approx K_{dg} (\Delta \omega_{m\_dg} - \Delta \omega_{bus}). \quad (6)$$

The small-signal model of (3) can be written as

$$\begin{aligned} -k_{p\_dg} \Delta \omega_{m\_dg} - \Delta P_{out\_dg} \\ = J_{dg} (\omega_{m\_dg} s \Delta \omega_{m\_dg} + s \Delta \omega_{m\_dg}^2) \\ + D_{dg} (\Delta \omega_{m\_dg} - \Delta \omega_{g\_dg}). \end{aligned} \quad (7)$$

As the frequency deviation from nominal frequency is relatively small,  $\omega_{m\_dg} s \Delta \omega_{m\_dg} \approx \omega_0 s \Delta \omega_{m\_dg}$ . Moreover, second-order perturbation terms can be neglected. Therefore, (7) becomes

$$\begin{aligned} -k_{p\_dg} \Delta \omega_{m\_dg} - \Delta P_{out\_dg} \\ = J_{dg} \omega_0 s \Delta \omega_{m\_dg} + D_{dg} (\Delta \omega_{m\_dg} - \Delta \omega_{g\_dg}). \end{aligned} \quad (8)$$

If line losses are neglected,  $\Delta P_{out\_dg} = \Delta P_{load}$ , where  $P_{load}$  is the active power consumed by the load. And if  $X_f \gg X_{line}$ ,  $\Delta \omega_{g\_dg} \approx \Delta \omega_{bus}$ . In this case, eliminate  $\Delta \omega_{g\_dg}$  and  $\Delta \omega_{bus}$  from (6) and (8), so that

$$\frac{\Delta \omega_{m\_dg}}{\Delta P_{load}} = -\frac{1 + (D_{dg}/K_{dg})s}{k_{p\_dg} + J_{dg} \omega_0 s}. \quad (9)$$

Equation (9) is the transfer function of frequency change over a small loading transition in stand-alone mode for a VSG. Let  $J_{dg} = 0$ ,  $D_{dg} = 0$ , and then the transfer function for a droop-control-based DG can be obtained as follows:

$$\frac{\Delta \omega_{m\_dg}}{\Delta P_{load}} = -\frac{1}{k_{p\_dg}}. \quad (10)$$

Let  $s = 0$  in (9), and then (9) is equivalent to (10). This implies that steady-state gain of (9) is determined by droop coefficient  $k_{p\_dg}$  and is independent of swing equation parameters. In other words, steady state of VSG control and droop control is the same if droop coefficients  $k_{p\_dg}$  are set equally.

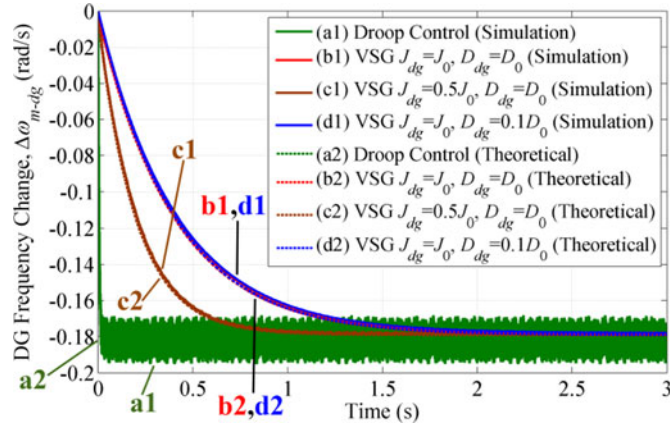


Fig. 3. Step responses of DG frequency during a loading transition in stand-alone mode with various parameters.

TABLE I  
PARAMETERS OF STAND-ALONE MODE

Parameter	Value	Parameter	Value
$E_{dg}$	6.6 kV	$k_{p\_dg}^*$	20 p.u.
$S_{base\_dg}$	1 MVA	$X_f$	0.1298 p.u.
$P_{0\_dg}$	1 p.u.	$X_{line}$	0.0076 p.u.
$\omega_0$	376.99 rad/s	$\delta_{dg}$	0
$J_0$	56.3 kg·m <sup>2</sup>	$V_{bus}$	6.57 kV
$D_0^*$	17 p.u.	$\Delta P_{load}$	0.0095 MW

It is possible to calculate step responses of DG frequency change during a small loading transition through (9) and (10) with various parameters, and the results are shown in Fig. 3 (dotted lines) along with corresponding simulation results (solid lines) obtained with PSCAD/EMTDC. Parameters used for both theoretical calculation and simulation are the same, as listed in Table I, except line resistance is taken into consideration in the simulation, as shown in Fig. 2(b).

As it is demonstrated in Fig. 3, in all cases, simulation results almost overlap corresponding theoretical results; thus, it can be concluded that the small-signal models are verified. Ripples can be observed in simulation result of droop control due to ripples in measured output power  $\Delta P_{out\_dg}$ . Normally, a filter should be applied to filter this ripple and its effect is discussed in Section III-C. To understand dynamic response of basic droop control without the filter, only a first-order filter with small time constant at 0.005 s is applied in simulation and experiment except other value is specified.

As for the comparison between each case, the frequency of VSG control changes slowly, whereas that of droop control suffers a step change. This implies that DG with VSG control has inertia thanks to the swing equation, and that DG with droop control has nearly no inertia. Moreover, larger value of  $J_{dg}$  results in slower frequency change, which indicates that inertia of the DG is determined by  $J_{dg}$ . On the other hand,  $D_{dg}$  has barely any influence on dynamic response in this situation. Besides, steady states of all cases are the same. This verifies previous conclusion that steady states only depend on  $k_{p\_dg}$ .

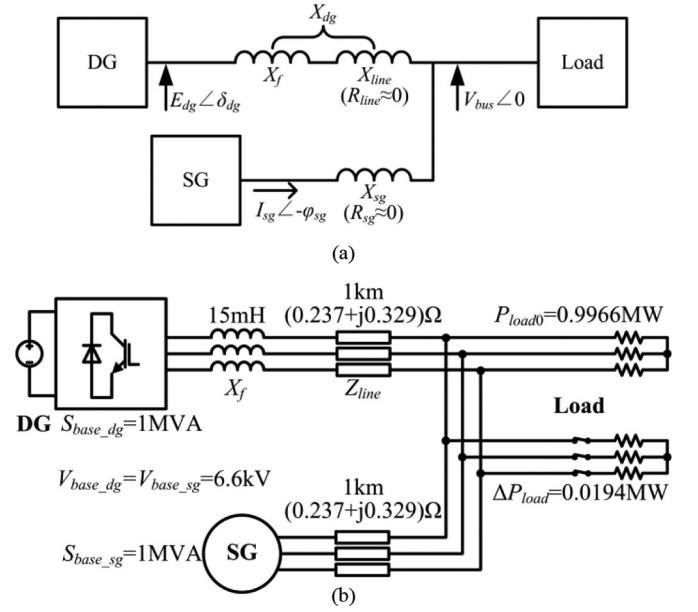


Fig. 4. (a) SG-connected mode model. (b) Simulation circuit of SG-connected mode.

### B. SG-Connected Mode

In this part, an SG-connected system shown in Fig. 4(a) is studied to show the importance of inertia in a network with high penetration level of inverter-based DG. It is assumed the penetration rate of DG in this network is up to 50%, and the rest of power generation comes from SG. In this case, it is preferred to study the rotor frequency change of SG rather than that of DG because the former is considered as the dominant one.

From the law of conservation of energy

$$\Delta P_{out\_dg} + \Delta P_{out\_sg} = \Delta P_{load} \quad (11)$$

where subscript “sg” indicates parameters related to SG.

Let  $\frac{\Delta P_{out\_dg}}{\Delta \omega_{bus}} = A$  and  $\frac{\Delta P_{out\_sg}}{\Delta \omega_{bus}} = B$ , so that (11) becomes

$$\Delta P_{out\_sg} (1 + A/B) = \Delta P_{load}. \quad (12)$$

The same equation as (6) holds for SG

$$s \Delta P_{out\_sg} \approx K_{sg} (\Delta \omega_{m\_sg} - \Delta \omega_{bus}). \quad (13)$$

Eliminate  $\Delta P_{out\_sg}$  from (12) and (13), so that

$$\frac{\Delta \omega_{m\_sg}}{\Delta P_{load}} = \frac{K_{sg} + Bs}{K_{sg}(A + B)}. \quad (14)$$

Now if  $A$  and  $B$  are known, the required transfer function can be obtained.

Eliminate  $\Delta \omega_{m\_dg}$  from (6) and (8), and then

$$A = \frac{\Delta P_{out\_dg}}{\Delta \omega_{bus}} = -\frac{k_{p\_dg} + J_{dg} \omega_0 s}{1 + \frac{k_{p\_dg} + D_{dg}}{K_{dg}} s + \frac{J_{dg} \omega_0}{K_{dg}} s^2}. \quad (15)$$

Because SG has the same model as VSG, (15) is also true for SG

$$B = \frac{\Delta P_{out\_sg}}{\Delta \omega_{bus}} = -\frac{k_{p\_sg} + J_{sg} \omega_0 s}{1 + \frac{k_{p\_sg} + D_{sg}}{K_{sg}} s + \frac{J_{sg} \omega_0}{K_{sg}} s^2}. \quad (16)$$

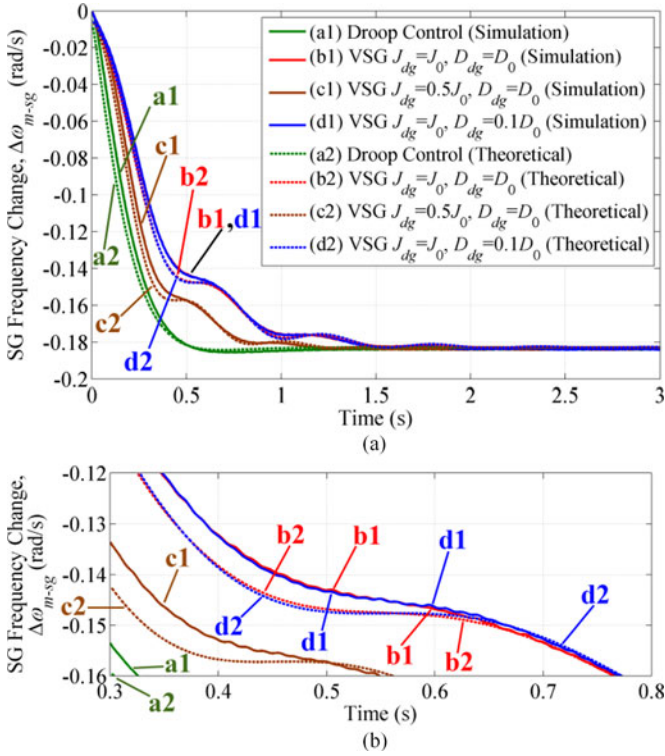


Fig. 5. (a) Step responses of SG frequency during a loading transition in SG-connected mode with various parameters. (b) Zoom in of (a).

TABLE II  
SG PARAMETERS

Parameter	Value	Parameter	Value
$V_{base-sg}$	6.6 kV	$X_q = X_q^l$	0.770 p.u.
$S_{base-sg}$	1 MVA	$X_q''$	0.375 p.u.
$P_{0-sg}$	1 p.u.	$T_d''$	0.0348 s
$\omega_0$	376.99 rad/s	$X_q''$	0.0346 s
$J_{sg}$	56.3 kg-m <sup>2</sup>	$T_{d-sg}$	0.1 s
$k_{p-sg}^*$	20 p.u.	$I_{sg}$	43.1 A
$X_{sg}$	0.0076 p.u.	$\varphi_{sg}$	0.00655 rad
$X_d$	1.90 p.u.	$V_{bus}$	6.57 kV
$X_d^l$	0.314 p.u.	$\Delta P_{load}$	0.0194 MW
$X_d''$	0.280 p.u.		

Let  $J_{dg} = 0, D_{dg} = 0$  in (15), and then  $A$  for droop control can be obtained as

$$A = \frac{\Delta P_{out-dg}}{\Delta\omega_{bus}} = -\frac{k_{p-dg}}{1 + (k_{p-dg}/K_{dg})s}. \quad (17)$$

However, for SG,  $K_{sg}$  and  $D_{sg}$  are not constant. They can be calculated from SG parameters and measurement data of  $V_{bus}$ ,  $I_{sg}$  (output current of SG), and  $\varphi_{sg}$  (phase difference between  $V_{bus}$  and  $I_{sg}$ ) [53].

Based on (14)–(17), it is possible to calculate the step responses of SG frequency change during a small loading transition, and the results are shown in Fig. 5 along with corresponding simulation results. (Note that for the calculation of  $B$ , (21) is used instead of (16), which is explicated in next part of this section.) Parameters of SG are listed in Table II, and parameters

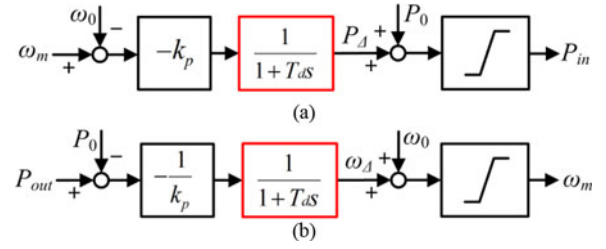


Fig. 6. (a) Governor of VSG control. (b)  $P$  droop controller of droop control.

of DG are the same as those in Table I. Simulation circuit is shown in Fig. 4(b), in which line resistance is included.

As shown in Fig. 5, simulation results verify theoretical results obtained with the small-signal model, although slight delay during first 0.5 s is observed. It is probably because in simulation, the input disturbance  $\Delta P_{load}$ , which is realized by switching on additional load, is not an ideal step due to the existence of line reactance. It can also be noted that the amplitude of oscillations in simulation results are slightly smaller than that in theoretical results, probably because simulation circuits include line resistance, which provides additional damping to the system. Like in stand-alone mode, it is demonstrated that DG with VSG control can contribute more inertia to the system than DG with droop control, since  $df/dt$  of the former is slower. Also, larger value of  $J_{dg}$  still increases the inertia of the system. In addition, system with larger  $D_{dg}$  has slightly smaller oscillation. Similarly, parameters of swing equation have no influence on steady state.

### C. Effects of Delays in Governor and $P$ Droop Controller

It is known that there is always a large delay in the mechanical governor of SG. In previous researches on VSG, this delay is also imitated when (2) is applied [39], [40], [42], as is shown in Fig. 6(a). For droop control, a low-pass filter is usually added into  $P$  droop controller to filter noises in the measured output power  $P_{out}$ , as is shown in Fig. 6(b). Assuming both delays are first-order lags with a time constant  $T_d$ ,  $k_p$  has to be replaced by  $k_p/(1+T_d s)$  for VSG control, and by  $k_p(1+T_d s)$  for droop control in the small-signal models. This difference is caused by the inverse of input and output in  $P$ - $\omega$  droop regulation. In VSG control, the input is active power and the output is frequency, whereas in droop control, it is the opposite, as illustrated in Fig. 6.

If this effect is taken into account for VSG, in stand-alone mode, (9) has to be modified as

$$\frac{\Delta\omega_{m-dg}}{\Delta P_{load}} = -\frac{1 + \left(T_{d-dg} + \frac{D_{dg}}{K_{dg}}\right)s + \frac{D_{dg}T_{d-dg}}{K_{dg}}s^2}{k_{p-dg} + J_{dg}\omega_0 s + J_{dg}\omega_0 T_{d-dg} s^2}. \quad (18)$$

and for droop control, (10) becomes

$$\frac{\Delta\omega_{m-dg}}{\Delta P_{load}} = -\frac{1}{k_{p-dg} + T_{d-dg}k_{p-dg}s}. \quad (19)$$

Meanwhile, in SG-connected mode, for VSG and SG, (15) and (16) have to be modified as (20) and (21) as shown bottom of the next page

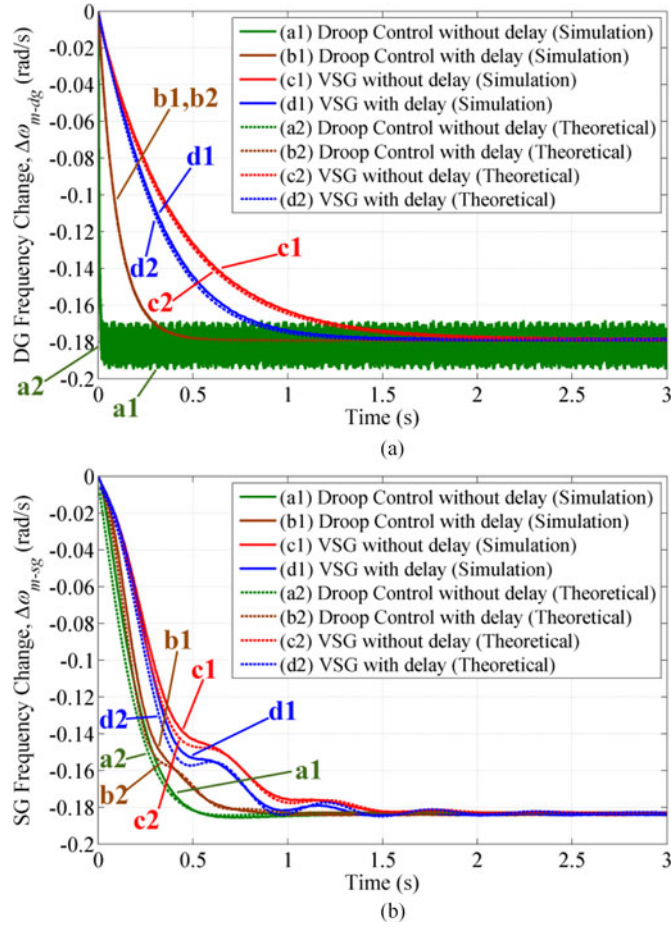


Fig. 7. Effects of delays on step responses of (a) DG or (b) SG frequency during a loading transition in (a) stand-alone mode and (b) SG-connected mode.

and for droop control, (17) becomes

$$A = -\frac{k_{p\_dg} + k_{p\_dg}T_{d\_dg}s}{1 + (k_{p\_dg}/K_{dg})s + (k_{p\_dg}T_{d\_dg}/K_{dg})s^2}. \quad (22)$$

Based on (18)–(22), step responses of frequency can be recalculated and then compared with cases without consideration of delays, as shown in Fig. 7. The time constant  $T_{d\_dg}$  is assumed to be 0.1 s. Simulation results are also provided in Fig. 7 to verify calculated theoretical results.

Fig. 7 illustrates the point that inverse of input and output in  $P$ - $\omega$  droop results in different effect of delay for each control method. The delay makes the frequency of systems with VSG control change faster, but makes that of systems with droop control change more slowly in both stand-alone mode and SG-connected mode. That is to say, the delay has a positive effect on droop control but a negative effect on VSG.

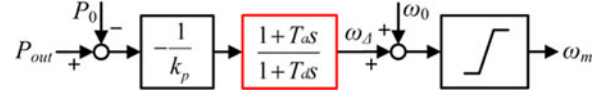


Fig. 8.  $P$  droop controller of droop control with a first-order lead-lag unit.

#### D. Inertial Droop Control

It is interesting to compare (9) with (19), and (15) with (22). If  $T_{d\_dg}$  is increased up to

$$T_{d\_dg} = J_{dg}\omega_0/k_{p\_dg} \quad (23)$$

the only difference between (9) and (19), or (15) with (22) is that the equations of VSG control have terms coming from  $D_{dg}$ , whereas those of droop control do not. That is to say, by adding a first-order lag unit, with time constant  $T_{d\_dg}$  specified by (23), into  $P$  droop controller, droop control can imitate the performance of VSG with a moment of inertia equal to  $J_{dg}$ .

Furthermore, if a first-order lead unit is also added into  $P$  droop controller, as shown in Fig. 8, (19) and (22) become

$$\frac{\Delta\omega_{m\_dg}}{\Delta P_{load}} = -\frac{1 + T_{a\_dg}s}{k_{p\_dg} + T_{d\_dg}k_{p\_dg}s} \quad (24)$$

$$A = -\frac{k_{p\_dg} + k_{p\_dg}T_{d\_dg}s}{1 + (k_{p\_dg}/K_{dg} + T_{a\_dg})s + (k_{p\_dg}T_{d\_dg}/K_{dg})s^2} \quad (25)$$

respectively. If the time constant is set to

$$T_{a\_dg} = D_{dg}/K_{dg} \quad (26)$$

then (24) is equivalent to (9), and (25) is equivalent to (15).

This conclusion is proved by Fig. 9 with both simulation results and calculated theoretical results. By adding a first-order lag unit with time constant specified by (23), droop control results in similar step response to VSG control, with slightly larger oscillation due to lack of damping factor. Additionally, when a first-order lead unit with time constant specified by (26) is also added, droop control leads to exactly the same step response as VSG control in theoretical results. Although in simulation results, there is still slight difference between the result of droop control with specified lead-lag unit (c1) and that of VSG (d1), probably due to the presence of line resistance, the damping effect of lead unit is confirmed by comparing line (b1) and line (c1). This implies that during small disturbance, VSG can be approximated by droop control, with a first-order lag unit to simulate inertia, and with a first-order lead unit to simulate damping factor. Although similar conclusion on the relation between first-order lag unit and inertia is mentioned

$$A = -\frac{k_{p\_dg} + J_{dg}\omega_0s + T_{d\_dg}J_{dg}\omega_0s^2}{1 + \left(T_{d\_dg} + \frac{k_{p\_dg} + D_{dg}}{K_{dg}}\right)s + \frac{T_{d\_dg}D_{dg} + J_{dg}\omega_0}{K_{dg}}s^2 + \frac{T_{d\_dg}J_{dg}\omega_0}{K_{dg}}s^3} \quad (20)$$

$$B = -\frac{k_{p\_sg} + J_{sg}\omega_0s + T_{d\_sg}J_{sg}\omega_0s^2}{1 + \left(T_{d\_sg} + \frac{k_{p\_sg} + D_{sg}}{K_{sg}}\right)s + \frac{T_{d\_sg}D_{sg} + J_{sg}\omega_0}{K_{sg}}s^2 + \frac{T_{d\_sg}J_{sg}\omega_0}{K_{sg}}s^3} \quad (21)$$

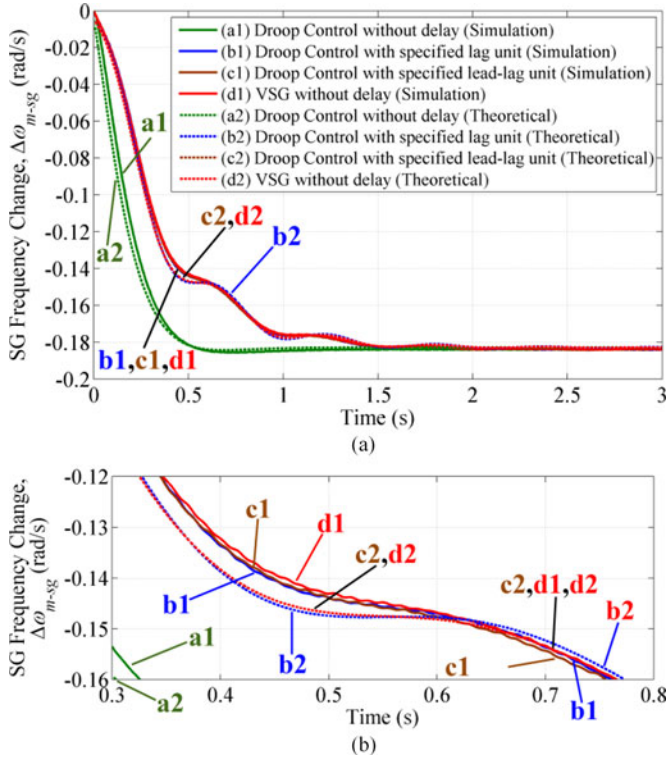


Fig. 9. (a) Step responses of SG frequency during a loading transition in SG-connected mode with specified lag or lead-lag unit in droop control. (b) Zoom in of (a).

in [50] and [51], the relation between first-order lead unit and damping factor has not been discussed in the literature.

#### IV. COMPARISONS OF ACTIVE POWER OSCILLATION

To compare the oscillation of output active power, state-space models of SG-connected mode are built, for both VSG and droop control, based on small-signal relations developed in Section III

$$\begin{cases} \dot{\mathbf{x}} = \mathbf{A}\mathbf{x} + \mathbf{B}\mathbf{u} \\ \mathbf{y} = \mathbf{C}\mathbf{x} + \mathbf{D}\mathbf{u} \end{cases} \quad (27)$$

where

$$\mathbf{u} = [\Delta P_{load}] \quad (28)$$

$$\mathbf{y} = [\Delta\omega_{m\_sg} \quad \Delta\omega_{m\_dg} \quad \Delta P_{out\_sg} \quad \Delta P_{out\_dg}]^T \quad (29)$$

and other matrices are listed as follows. For VSG control: (33) and (34) as shown bottom of the next page

$$\mathbf{x} = \begin{bmatrix} \Delta\omega_{m\_sg} + \frac{D_{sg}}{J_{sg}\omega_0(K_{sg} + K_{dg})}\Delta P_{load} \\ \Delta\omega_{m\_dg} + \frac{D_{dg}}{J_{dg}\omega_0(K_{sg} + K_{dg})}\Delta P_{load} \\ \Delta\delta_{sg} - \frac{1}{K_{sg} + K_{dg}}\Delta P_{load} \\ \Delta P_{in\_sg} \\ \Delta P_{in\_dg} \end{bmatrix} \quad (30)$$

$$\mathbf{C} = \begin{bmatrix} 1 & 0 & 0 & 0 & 0 \\ 0 & 1 & 0 & 0 & 0 \\ 0 & 0 & K_{sg} & 0 & 0 \\ 0 & 0 & -K_{sg} & 0 & 0 \end{bmatrix} \quad (31)$$

$$\mathbf{D} = \begin{bmatrix} \frac{D_{sg}}{J_{sg}\omega_0(K_{sg} + K_{dg})} \\ \frac{D_{dg}}{J_{dg}\omega_0(K_{sg} + K_{dg})} \\ \frac{K_{sg}}{K_{sg} + K_{dg}} \\ \frac{K_{dg}}{K_{sg} + K_{dg}} \end{bmatrix} \quad (32)$$

For droop control: (38) and (39) as shown bottom of the next page

$$\mathbf{x} = \begin{bmatrix} \Delta\omega_{m\_sg} + \frac{D_{sg}}{J_{sg}\omega_0(K_{sg} + K_{dg})}\Delta P_{load} \\ \Delta\omega_{m\_dg} \\ \Delta\delta_{sg} - \frac{1}{K_{sg} + K_{dg}}\Delta P_{load} \\ \Delta P_{in\_sg} \end{bmatrix} \quad (35)$$

$$\mathbf{C} = \begin{bmatrix} 1 & 0 & 0 & 0 \\ 0 & 1 & 0 & 0 \\ 0 & 0 & K_{sg} & 0 \\ 0 & 0 & -K_{sg} & 0 \end{bmatrix} \quad (36)$$

$$\mathbf{D} = \begin{bmatrix} \frac{D_{sg}}{J_{sg}\omega_0(K_{sg} + K_{dg})} \\ 0 \\ \frac{K_{sg}}{K_{sg} + K_{dg}} \\ \frac{K_{dg}}{K_{sg} + K_{dg}} \end{bmatrix} \quad (37)$$

It can be proved that the transfer function of the first output  $\Delta\omega_{m\_sg}$  over the input  $\Delta P_{load}$  deduced from this state-space model is the same as that described by (14), (20), and (21).

Since oscillations in output variables, including DG output power  $\Delta P_{out\_dg}$ , are determined by the eigenvalues of state matrix  $\mathbf{A}$ , it is important to analyze how these eigenvalues vary according to different parameters, as shown in Fig. 10. In each diagram, radial lines indicate damping ratio  $\zeta$ , whereas circle lines indicate nature frequency  $\omega_n$ . Parameters used for calculation are the same as those listed in Tables I and II.

It is implied that VSG control is more oscillatory than droop control due to smaller  $\zeta$  of the complex conjugate eigenvalues. Although oscillation in output power is a common phenomenon

in SG, it may cause overcurrent in DG and stop the inverter, because an inverter usually has weaker overload ability than a SG of same rating. However, this problem can be solved by increasing damping factor  $D_{dg}$  and/or line reactance  $X_{dg}$ , as  $\zeta$  of the complex conjugate eigenvalues increases in these cases as it is shown in Fig. 10. For example, a well-designed damping method based on modification of  $D_{dg}$  and considering line

resistance is presented in [41]. As for  $X_{dg}$ , it can be increased by virtual impedance control, which is mentioned in [11]–[13], [31], and [32], but for the purpose of decoupling active and reactive power. Detailed study on this point is a future work and is beyond the scope of this paper.

In addition, it is shown that  $J_{dg}$  affects the oscillation frequency  $\omega_d$ , which is indicated by the distance between the

$$\mathbf{A} = \begin{bmatrix} -\frac{D_{sg}K_{dg}}{J_{sg}\omega_0(K_{sg}+K_{dg})} & \frac{D_{sg}K_{dg}}{J_{sg}\omega_0(K_{sg}+K_{dg})} & -\frac{K_{sg}}{J_{sg}\omega_0} & \frac{1}{J_{sg}\omega_0} & 0 \\ \frac{D_{dg}K_{sg}}{J_{dg}\omega_0(K_{sg}+K_{dg})} & -\frac{D_{dg}K_{sg}}{J_{dg}\omega_0(K_{sg}+K_{dg})} & \frac{K_{sg}}{J_{dg}\omega_0} & 0 & \frac{1}{J_{dg}\omega_0} \\ \frac{K_{dg}}{K_{sg}+K_{dg}} & -\frac{K_{dg}}{K_{sg}+K_{dg}} & 0 & 0 & 0 \\ -\frac{k_{p-sg}}{T_{d-sg}} & 0 & 0 & -\frac{1}{T_{d-sg}} & 0 \\ 0 & -\frac{k_{p-dg}}{T_{d-dg}} & 0 & 0 & -\frac{1}{T_{d-dg}} \end{bmatrix} \quad (33)$$

$$\mathbf{B} = \begin{bmatrix} -\frac{K_{sg}}{J_{sg}\omega_0(K_{sg}+K_{dg})} - \frac{D_{sg}D_{dg}K_{dg}}{J_{sg}J_{dg}\omega_0^2(K_{sg}+K_{dg})^2} + \frac{D_{sg}^2K_{dg}}{J_{sg}^2\omega_0^2(K_{sg}+K_{dg})^2} \\ -\frac{1}{J_{dg}\omega_0} + \frac{K_{sg}}{J_{dg}\omega_0(K_{sg}+K_{dg})} - \frac{D_{sg}D_{dg}K_{sg}}{J_{sg}J_{dg}\omega_0^2(K_{sg}+K_{dg})^2} + \frac{D_{dg}^2K_{sg}}{J_{dg}^2\omega_0^2(K_{sg}+K_{dg})^2} \\ -\frac{D_{sg}K_{dg}}{J_{sg}\omega_0(K_{sg}+K_{dg})^2} + \frac{D_{dg}K_{dg}}{J_{dg}\omega_0(K_{sg}+K_{dg})^2} \\ \frac{k_{p-sg}D_{sg}}{T_{d-sg}J_{sg}\omega_0(K_{sg}+K_{dg})} \\ \frac{k_{p-dg}D_{dg}}{T_{d-dg}J_{dg}\omega_0(K_{sg}+K_{dg})} \end{bmatrix} \quad (34)$$

$$\mathbf{A} = \begin{bmatrix} -\frac{D_{sg}K_{dg}}{J_{sg}\omega_0(K_{sg}+K_{dg})} & \frac{D_{sg}K_{dg}}{J_{sg}\omega_0(K_{sg}+K_{dg})} & -\frac{K_{sg}}{J_{sg}\omega_0} & \frac{1}{J_{sg}\omega_0} \\ 0 & -\frac{1}{T_{d-dg}} & \frac{K_{sg}}{k_{p-dg}T_{d-dg}} & 0 \\ \frac{K_{dg}}{K_{sg}+K_{dg}} & -\frac{K_{dg}}{K_{sg}+K_{dg}} & 0 & 0 \\ -\frac{k_{p-sg}}{T_{d-sg}} & 0 & 0 & -\frac{1}{T_{d-sg}} \end{bmatrix} \quad (38)$$

$$\mathbf{B} = \begin{bmatrix} -\frac{K_{sg}}{J_{sg}\omega_0(K_{sg}+K_{dg})} + \frac{D_{sg}^2K_{dg}}{J_{sg}^2\omega_0^2(K_{sg}+K_{dg})^2} \\ -\frac{1}{k_{p-dg}T_{d-dg}} + \frac{K_{sg}}{k_{p-dg}T_{d-dg}(K_{sg}+K_{dg})} \\ -\frac{D_{sg}K_{dg}}{J_{sg}\omega_0(K_{sg}+K_{dg})^2} \\ \frac{k_{p-sg}D_{sg}}{T_{d-sg}J_{sg}\omega_0(K_{sg}+K_{dg})} \end{bmatrix} \quad (39)$$

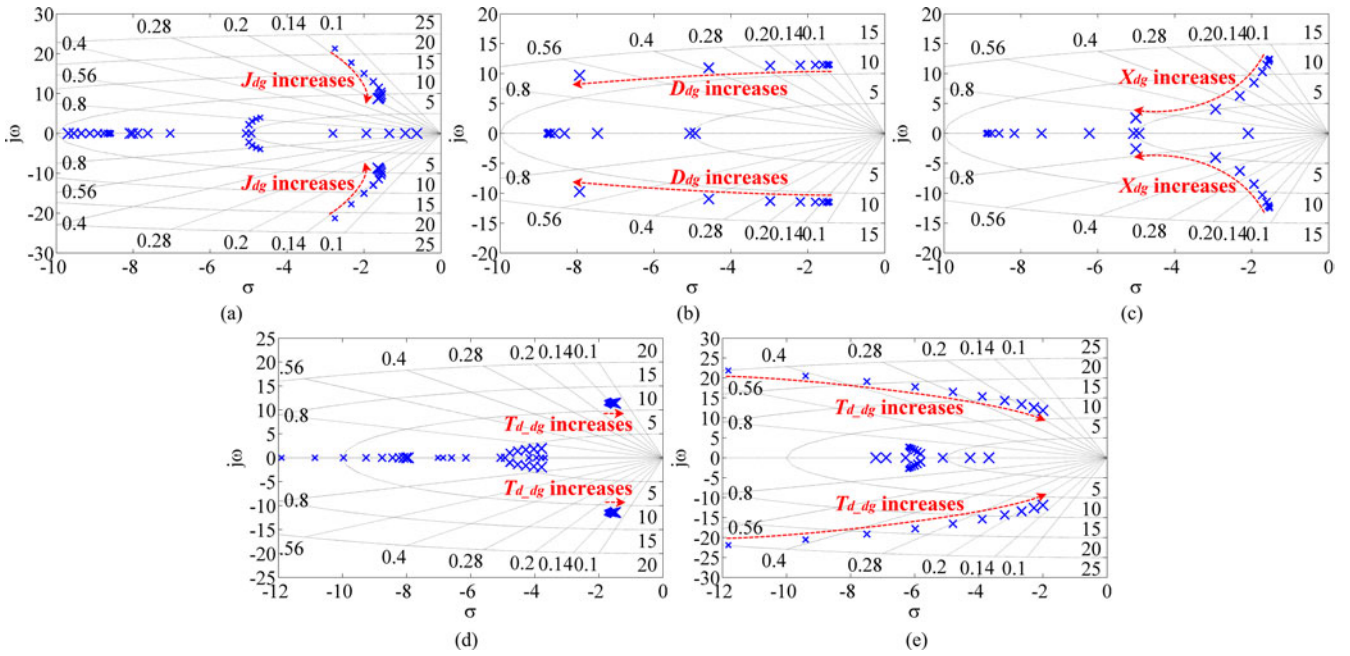


Fig. 10. Eigenvalues when (a)  $J_{dg}$  of VSG varies from  $1.5^{-4}J_0$  to  $1.5^5J_0$ , (b)  $D_{dg}$  of VSG varies from  $2^{-4}D_0$  to  $2^5D_0$ , (c)  $X_{dg}$  of VSG varies from  $2.5^{-4} \times 0.1374$  to  $2.5^5 \times 0.1374$  p.u., (d)  $T_{d,dg}$  of VSG varies from  $1.09^{-4} \times 0.1$  to  $1.09^5 \times 0.1$  s, and (e)  $T_{d,dg}$  of droop control varies from  $1.25^{-4} \times 0.1$  to  $1.25^5 \times 0.1$  s.

eigenvalues and the real axis, but has barely any effect on the damping ratio. It is also shown that the increase of  $T_{d,dg}$  not only results in higher  $df/dt$  as discussed in last section, but also makes the system more oscillatory. Therefore, it is better not to simulate governor delay in VSG control.

Droop control may also become oscillatory if the lag time constant  $T_{d,dg}$  is very large. In this case, its distribution of eigenvalues becomes similar to that of VSG control. This verifies the conclusion in last section, that droop control can be used to simulate VSG by increasing  $T_{d,dg}$ .

Moreover, for both control methods, no matter how parameters change, no right-half-plan pole is observed. This implies that parameters evaluated in this paper do not influence the stability of active power control in SG-connected mode.

V. EXPERIMENTAL RESULTS

Scale-down experiments are also executed to support the points in Section III. Experimental circuits of stand-alone mode and of SG-connected mode are shown in Fig. 11(a) and (b), respectively. Three-phase power supply rectified by a diode bridge is used to imitate the dc output of a DG. The block “transmission line (TU)” in these graphs is a  $\Pi$  circuit to simulate a section of 40 km HV transmission line, which is demonstrated in Fig. 12. Parameters of stand-alone mode and of SG-connected mode are listed in Tables III and IV, and the results of stand-alone mode and SG-connected mode are shown in Figs. 13 and 14, respectively.

For stand-alone mode, experimental results (solid lines) coincide with corresponding theoretical results (dotted lines). This proves again that the small-signal models and the conclusions discussed in Section III are correct.

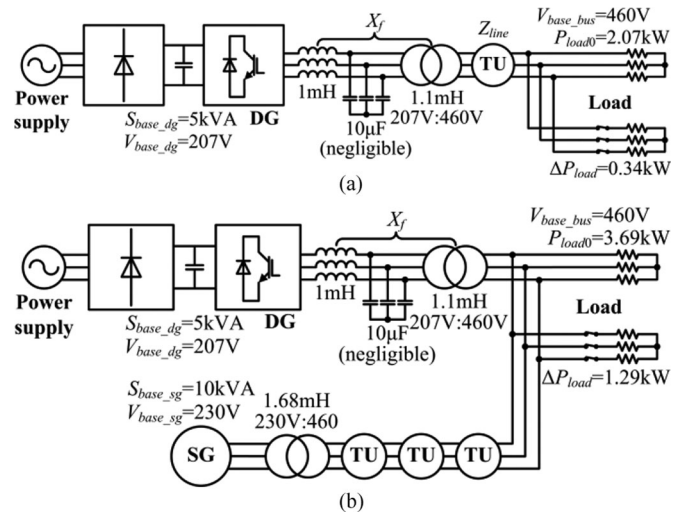


Fig. 11. Experimental circuit of (a) stand-alone mode and (b) SG-connected mode.

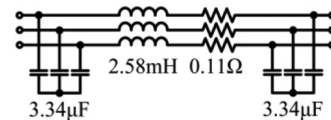


Fig. 12. TU.

For SG-connected mode, by comparing experimental results, the same conclusions can be drawn as those in Section III. In Fig. 14(a), system with VSG control still results in slower frequency change than that with droop control, and the frequency changes faster when  $J_{dg}$  decreases. In Fig. 14(b), it can still be noticed that the delay ( $T_{d,dg} = 0.1$  s) makes the frequency

TABLE III  
EXPERIMENTAL PARAMETERS OF STAND-ALONE MODE

Parameter	Value	Parameter	Value
$E_{dg}$	207 V	$J_0$	0.2815 kg · m <sup>2</sup>
$S_{base\_dg}$	5 kVA	$D_0^*$	17 p.u.
$P_{0\_dg}$	1 p.u.	$\delta_{dg}$	0
$\omega_0$	376.99 rad/s	$V_{bus}$	447.05 V
$k_{p\_dg}^*$	20 p.u.	$\Delta P_{load}$	0.34 kW

TABLE IV  
EXPERIMENTAL PARAMETERS OF SG-CONNECTED MODE

Parameter	Value	Parameter	Value
$V_{base\_sg}$	230 V	$X_q$	1.31 p.u.
$S_{base\_sg}$	10 kVA	$X'_q$	0.55 p.u.
$P_{0\_sg} = P_{0\_dg}$	0 p.u.	$X''_q$	0.27 p.u.
$\omega_0$	376.99 rad/s	$T'_d$	0.01 s
$J_{sg}$	0.563 kg · m <sup>2</sup>	$T''_q$	0.02 s
$k_{p\_sg}^*$	20 p.u.	$I_{sg}$	4.77 A
$X_d$	1.35 p.u.	$\varphi_{sg}$	0.76 rad
$X'_d$	0.48 p.u.	$V_{bus}$	454.8 V
$X''_d$	0.27 p.u.	$\Delta P_{load}$	1.29 kW

Other DG parameters are the same as those in Table III

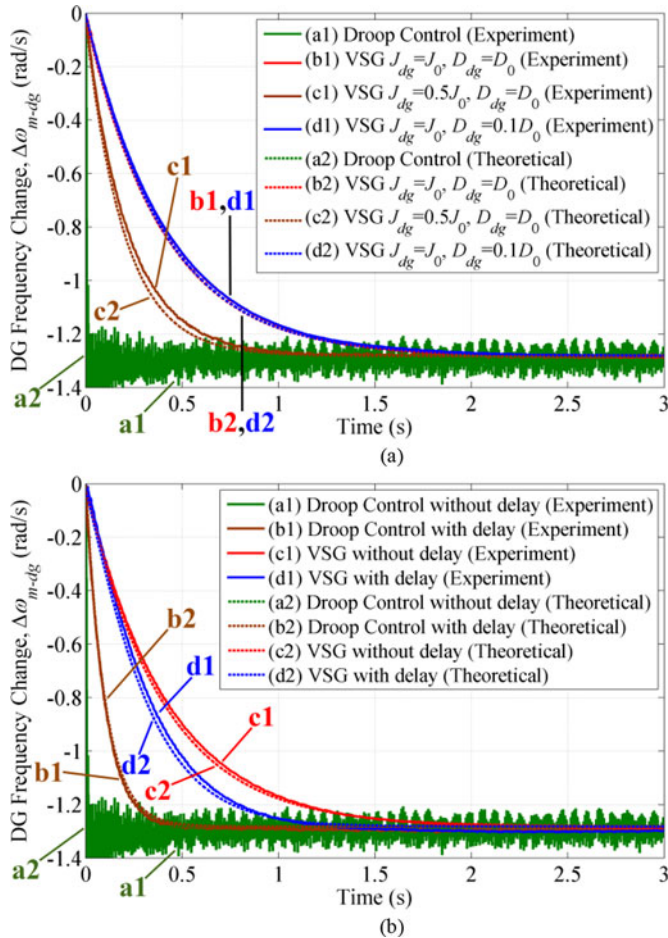


Fig. 13. Experimental results of stand-alone mode to verify (a) effects of parameters and (b) effects of delays.

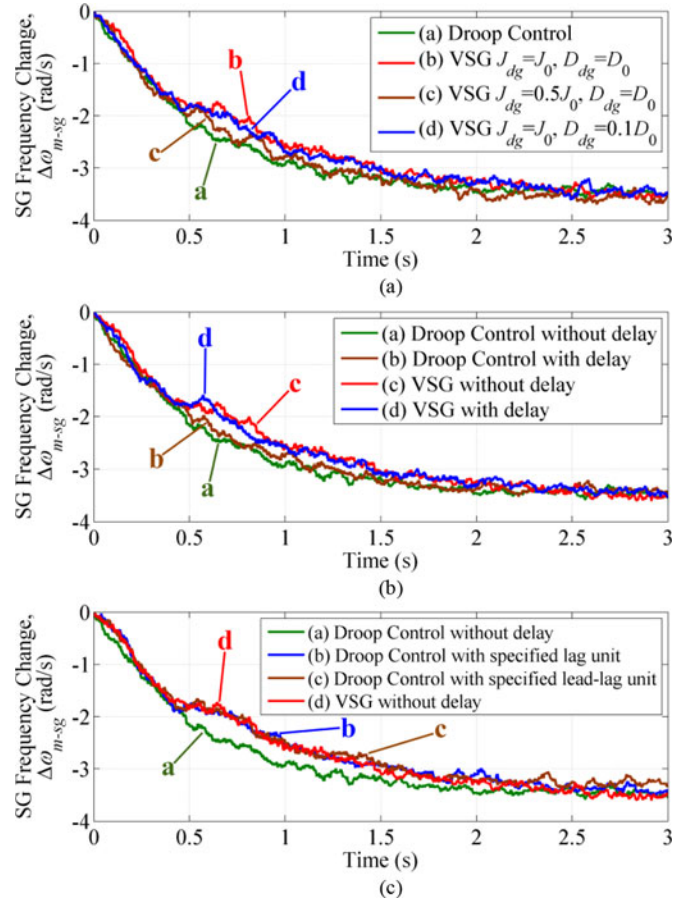


Fig. 14. Experimental results of SG-connected mode to verify (a) effects of parameters, (b) effects of delays, and (c) inertial droop control.

change faster in VSG control, but makes the frequency change more slowly in droop control. Similarly, in Fig. 14(c), with specified lag unit or lead-lag unit, droop control has similar dynamic response to VSG. Although in experimental results, it is difficult to confirm the difference in amplitude of oscillations due to noises and insufficient measurement resolution, simulation results are sufficient to confirm authors' points.

## VI. CONCLUSION

In this paper, small-signal models of VSG control and of droop control were built, for both stand-alone mode and SG-connected mode, to compare the dynamic responses of the two control methods. All results were verified by simulations and experiments. Oscillation phenomena were studied through state-space models. Results are summarized as follows.

- 1) It was demonstrated that VSG has larger inertia than droop control and therefore better frequency stability, and the amount of inertia depends on virtual moment of inertia  $J$  whereas the damping ratio depends on damping factor  $D$  and output reactance  $X$ . It was also proved that the delay in governor of VSG reduces the inertia and amplifies oscillation. As a result, it was suggested to remove

governor delay from VSG control. Contrarily, delay in  $P$  droop controller of droop control can increase the inertia.

- 2) It was shown that droop control with a well-designed first-order lead-lag unit in  $P$  droop controller has equivalent small-signal model to that of VSG control. This modified droop control, which can be called inertial droop control, provides a novel solution of virtual inertia, which is more familiar to engineers working on UPS and microgrid applications.
- 3) It was also pointed out that the output active power of VSG is more oscillatory than that of droop control, but this problem can be resolved by tuning the damping factor and/or the output reactance. Besides, it was proved that active power controls of both VSG control and droop control are stable.
- 4) It was shown that VSG control and proposed inertial droop control inherit the advantages of droop control, and in addition, provides inertia support for the system. This implies that in the applications where inertia is an important index, e.g., in microgrids, VSG control and proposed inertial droop control have the potential to replace conventional inertia-less droop control.
- 5) The small-signal models and state-space models presented in this paper provide novel analytical approaches for understanding the dynamic characteristics of VSG and droop control, which may stimulate new ideas on improving dynamic performances of both control methods.

#### REFERENCES

- [1] F. Blaabjerg, R. Teodorescu, M. Liserre, and A. V. Timbus, "Overview of control and grid synchronization for distributed power generation systems," *IEEE Trans. Ind. Electron.*, vol. 53, no. 5, pp. 1398–1409, Oct. 2006.
- [2] M. C. Chandorkar, D. M. Divan, and R. Adapa, "Control of parallel connected inverters in standalone ac supply systems," *IEEE Trans. Ind. Appl.*, vol. 29, no. 1, pp. 136–143, Jan./Feb. 1993.
- [3] K. Debrabandere, B. Bolsens, J. Van Den Keybus, A. Woyte, J. Driesen, and R. Belmans, "A voltage and frequency droop control method for parallel inverters," *IEEE Trans. Power Electron.*, vol. 22, no. 4, pp. 1107–1115, Jul. 2007.
- [4] H. Nikkhajoei and R. H. Lasseter, "Distributed generation interface to the CERTS microgrid," *IEEE Trans. Power Del.*, vol. 24, no. 3, pp. 1598–1608, Jul. 2009.
- [5] A. Engler and N. Sultanis, "Droop control in LV-grids," in *Proc. Int. Conf. Future Power Syst.*, 2005, pp. 1–6.
- [6] J. M. Guerrero, J. Matas, L. G. De Vicuna, M. Castilla, and J. Miret, "Decentralized control for parallel operation of distributed generation inverters using resistive output impedance," *IEEE Trans. Ind. Electron.*, vol. 54, no. 2, pp. 994–1004, Apr. 2007.
- [7] T. L. Vandoorn, B. Meersman, L. Degroote, B. Renders, and L. Vandevelde, "A control strategy for islanded microgrids with dc-link voltage control," *IEEE Trans. Power Del.*, vol. 26, no. 2, pp. 703–713, Apr. 2011.
- [8] T. L. Vandoorn, B. Meersman, J. D. M. De Koning, and L. Vandevelde, "Analogy between conventional grid control and islanded microgrid control based on a global DC-link voltage droop," *IEEE Trans. Power Del.*, vol. 27, no. 3, pp. 1405–1414, Jul. 2012.
- [9] Y. Li and Y. W. Li, "Power management of inverter interfaced autonomous microgrid based on virtual frequency-voltage frame," *IEEE Trans. Smart Grid*, vol. 2, no. 1, pp. 30–40, Mar. 2011.
- [10] J. A. Peças Lopes, C. L. Moreira, and A. G. Madureira, "Defining control strategies for microgrids in islanded operation," *IEEE Trans. Power Syst.*, vol. 21, no. 2, pp. 916–924, May 2006.
- [11] J. C. Vasquez, J. M. Guerrero, M. Savaghebi, J. Eloy-Garcia, and R. Teodorescu, "Modeling, analysis, and design of stationary-reference-frame droop-controlled parallel three-phase voltage source inverters," *IEEE Trans. Ind. Electron.*, vol. 60, no. 4, pp. 1271–1280, Apr. 2013.
- [12] J. M. Guerrero, J. C. Vasquez, and R. Teodorescu, "Hierarchical control of droop-controlled DC and AC microgrids—A general approach towards standardization," *IEEE Trans. Ind. Electron.*, vol. 58, no. 1, pp. 158–172, Jan. 2011.
- [13] A. Bidram and A. Davoudi, "Hierarchical structure of microgrids control system," *IEEE Trans. Smart Grid*, vol. 3, no. 4, pp. 1963–1976, Dec. 2012.
- [14] Q. Shafiee, J. M. Guerrero, and J. C. Vasquez, "Distributed secondary control for islanded microgrids—A novel approach," *IEEE Trans. Power Electron.*, vol. 29, no. 2, pp. 1018–1031, Feb. 2014.
- [15] A. Micallef, M. Apap, C. Spiteri-Staines, J. M. Guerrero, and J. C. Vasquez, "Reactive power sharing and voltage harmonic distortion compensation of droop controlled single phase islanded microgrids," *IEEE Trans. Smart Grid*, vol. 5, no. 3, pp. 1149–1158, May 2014.
- [16] J. He and Y. W. Li, "An enhanced microgrid load demand sharing strategy," *IEEE Trans. Power Electron.*, vol. 27, no. 9, pp. 3984–3995, Sep. 2012.
- [17] J. He, Y. W. Li, and F. Blaabjerg, "An enhanced islanding microgrid reactive power, imbalance power, and harmonic power sharing scheme," *IEEE Trans. Power Electron.*, vol. 30, no. 6, pp. 3389–3401, Jun. 2015.
- [18] H. Mahmood, D. Michaelson, and J. Jiang, "Accurate reactive power sharing in an islanded microgrid using adaptive virtual impedances," *IEEE Trans. Power Electron.*, vol. 30, no. 3, pp. 1605–1617, Mar. 2015.
- [19] H. Han, Y. Liu, Y. Sun, M. Su, and J. M. Guerrero, "An improved droop control strategy for reactive power sharing in islanded microgrid," *IEEE Trans. Power Electron.*, vol. 30, no. 6, pp. 3133–3141, Jun. 2015.
- [20] J. He, Y. W. Li, J. M. Guerrero, F. Blaabjerg, and J. C. Vasquez, "An islanding microgrid power sharing approach using enhanced virtual impedance control scheme," *IEEE Trans. Power Electron.*, vol. 28, no. 11, pp. 5272–5282, Nov. 2013.
- [21] Y. W. Li and C.-N. Kao, "An accurate power control strategy for power-electronics-interfaced distributed generation units operating in a low-voltage multibus microgrid," *IEEE Trans. Power Electron.*, vol. 24, no. 12, pp. 2977–2988, Dec. 2009.
- [22] W. Yao, M. Chen, J. M. Guerrero, and Z.-M. Qian, "Design and analysis of the droop control method for parallel inverters considering the impact of the complex impedance on the power sharing," *IEEE Trans. Ind. Electron.*, vol. 58, no. 2, pp. 576–588, Feb. 2011.
- [23] Q.-C. Zhong, "Robust droop controller for accurate proportional load sharing among inverters operated in parallel," *IEEE Trans. Ind. Electron.*, vol. 60, no. 4, pp. 1281–1290, Apr. 2013.
- [24] C.-T. Lee, C.-C. Chu, and P.-T. Cheng, "A new droop control method for the autonomous operation of distributed energy resource interface converters," *IEEE Trans. Power Electron.*, vol. 28, no. 4, pp. 1980–1993, Apr. 2013.
- [25] Y. Zhu, Z. Fang, F. Wang, B. Liu, and Y. Zhao, "A wireless reactive power sharing strategy for islanded microgrid based on feeder current sensing," *IEEE Trans. Power Electron.*, to be published, DOI: 10.1109/TPEL.2014.2386851.
- [26] M. B. Delghavi and A. Yazdani, "Islanded-mode control of electronically coupled distributed-resource units under unbalanced and nonlinear load conditions," *IEEE Trans. Power Del.*, vol. 26, no. 2, pp. 661–673, Apr. 2011.
- [27] T.-L. Lee and P.-T. Cheng, "Design of a new cooperative harmonic filtering strategy for distributed generation interface converters in an islanding network," *IEEE Trans. Power Electron.*, vol. 22, no. 5, pp. 1919–1927, Sep. 2007.
- [28] J. Hu, J. Zhu, D. G. Dorrell, and J. M. Guerrero, "Virtual flux droop method—A new control strategy of inverters in microgrids," *IEEE Trans. Power Electron.*, vol. 29, no. 9, pp. 4704–4711, Sep. 2014.
- [29] I.-Y. Chung, W. Liu, D. A. Cartes, E. G. J. Collins, and S.-I. Moon, "Control methods of inverter-interfaced distributed generators in a microgrid system," *IEEE Trans. Ind. Appl.*, vol. 46, no. 3, pp. 1078–1088, May/Jun. 2010.
- [30] R. Majumder, B. Chaudhuri, A. Ghosh, R. Majumder, G. Ledwich, and F. Zare, "Improvement of stability and load sharing in an autonomous microgrid using supplementary droop control loop," *IEEE Trans. Power Syst.*, vol. 25, no. 2, pp. 796–808, May 2010.
- [31] J. M. Guerrero, L. García De Vicuña, J. Matas, M. Castilla, and J. Miret, "Output impedance design of parallel-connected UPS inverters with wireless load-sharing control," *IEEE Trans. Ind. Electron.*, vol. 52, no. 4, pp. 1126–1135, Aug. 2005.
- [32] J. M. Guerrero, L. Hang, and J. Uceda, "Control of distributed uninterruptible power supply systems," *IEEE Trans. Ind. Electron.*, vol. 55, no. 8, pp. 2845–2859, Aug. 2008.

- [33] J. Driesen and K. Visscher, "Virtual synchronous generators," in *Proc. IEEE Power Energy Soc. Gen. Meeting—Convers. Del. Elect. Energy 21st Century*, 2008, pp. 1–3.
- [34] M. P. N. Van Wessenbeek, S. W. H. De Haan, P. Varela, and K. Visscher, "Grid tied converter with virtual kinetic storage," in *Proc. IEEE Powertech Conf.*, 2009, pp. 1–7.
- [35] M. Torres and L. A. C. Lopes, "Virtual synchronous generator control in autonomous wind-diesel power systems," in *Proc. IEEE Elect. Power Energy Conf.*, 2009, pp. 1–6.
- [36] V. Karapanos, S. De Haan, and K. Zwetsloot, "Real time simulation of a power system with VSG hardware in the loop," in *Proc. 37th Annu. Conf. IEEE Ind. Electron. Soc.*, 2011, pp. 3748–3754.
- [37] X.-Z. Yang, J.-H. Su, M. Ding, J.-W. Li, and D. Yan, "Control strategy for virtual synchronous generator in microgrid," in *Proc. 4th Int. Conf. Elect. Utility Dereg. Restruct. Power Technol.*, 2011, pp. 1633–1637.
- [38] Y. Hirase, O. Noro, E. Yoshimura, H. Nakagawa, K. Sakimoto, and Y. Shindo, "Virtual synchronous generator control with double decoupled synchronous reference frame for single-phase inverter," in *Proc. Int. Power Electron. Conf.*, 2014, pp. 1552–1559.
- [39] K. Sakimoto, Y. Miura, and T. Ise, "Stabilization of a power system with a distributed generator by a virtual synchronous generator function," in *Proc. 8th IEEE Int. Conf. Power Electron.*, 2011, pp. 1498–1505.
- [40] T. Shintai, Y. Miura, and T. Ise, "Reactive power control for load sharing with virtual synchronous generator control," in *Proc. 7th Int. Power Electron. Motion Control Conf.*, 2012, pp. 846–853.
- [41] T. Shintai, Y. Miura, and T. Ise, "Oscillation damping of a distributed generator using a virtual synchronous generator," *IEEE Trans. Power Del.*, vol. 29, no. 2, pp. 668–676, Apr. 2014.
- [42] J. Alipoor, Y. Miura, and T. Ise, "Power system stabilization using virtual synchronous generator with alternating moment of inertia," *IEEE J. Emerg. Sel. Topics Power Electron.*, vol. 3, no. 2, pp. 451–458, Jun. 2015.
- [43] Y. Chen, R. Hesse, D. Turschner, and H.-P. Beck, "Improving the grid power quality using virtual synchronous machines," in *Proc. Int. Conf. Power Eng. Energy. Elect. Drives*, 2011, pp. 1–6.
- [44] Q.-C. Zhong and G. Weiss, "Synchronverters: Inverters that mimic synchronous generators," *IEEE Trans. Ind. Electron.*, vol. 58, no. 4, pp. 1259–1267, Apr. 2011.
- [45] Q.-C. Zhong, P.-L. Nguyen, Z. Ma, and W. Sheng, "Self-synchronized synchronverters: Inverters without a dedicated synchronization unit," *IEEE Trans. Power Electron.*, vol. 29, no. 2, pp. 617–630, Feb. 2014.
- [46] G. Delille, B. Francois, and G. Malarange, "Dynamic frequency control support by energy storage to reduce the impact of wind and solar generation on isolated power system's inertia," *IEEE Trans. Sustain. Energy*, vol. 3, no. 4, pp. 931–939, Oct. 2012.
- [47] M. A. Torres L., L. A. C. Lopes, L. A. Moran T., and J. R. Espinoza C., "Self-tuning virtual synchronous machine: A control strategy for energy storage systems to support dynamic frequency control," *IEEE Trans. Energy Convers.*, vol. 29, no. 4, pp. 833–840, Dec. 2014.
- [48] N. Soni, S. Doolla, and M. C. Chandorkar, "Improvement of transient response in microgrids using virtual inertia," *IEEE Trans. Power Del.*, vol. 28, no. 3, pp. 1830–1838, Jul. 2013.
- [49] A. D. Paquette, M. J. Reno, R. G Harley, and D. M. Divan, "Sharing transient loads: Causes of unequal transient load sharing in islanded microgrid operation," *IEEE Ind. Appl. Mag.*, vol. 20, no. 2, pp. 23–34, Mar./Apr. 2014.
- [50] M. Guan, W. Pan, J. Zhang, Q. Hao, J. Cheng, and X. Zheng, "Synchronous generator emulation control strategy for voltage source converter (VSC) stations," *IEEE Trans. Power Syst.*, vol. 30, no. 6, pp. 3093–3101, Nov. 2015.
- [51] Y. Du, J. M. Guerrero, L. Chang, J. Su, and M. Mao, "Modeling, analysis, and design of a frequency-droop-based virtual synchronous generator for microgrid applications," in *Proc. ECCE Asia Downunder*, 2013, pp. 643–649.
- [52] J. Liu, Y. Miura, and T. Ise, "Dynamic characteristics and stability comparisons between virtual synchronous generator and droop control in inverter-based distributed generators," in *Proc. Int. Power Electron. Conf.*, 2014, pp. 1536–1543.
- [53] J. Machowski, J. Bialek, and J. R. Bumby, *Power System Dynamics and Stability*. New York, NY, USA: Wiley, 1997, pp. 141–182.



**Jia Liu** (S'15) was born in Xuzhou, China, in 1986. He received the B.Eng. and M.Eng. degrees in electrical engineering from Xi'an Jiaotong University, Xi'an, China, in 2008 and 2011, respectively, and the Engineering degree in mechanical systems from the University of Technology of Troyes, Troyes, France, in 2011. He is currently working toward the Ph.D. degree at Osaka University, Osaka, Japan.

He was with Delta Electronics (Jiangsu), Ltd., China, from 2011 to 2012. His research interests include power converter control, microgrids, modular multilevel converters, and motor control.



**Yushi Miura** (M'06) received the Doctoral degree in electrical and electronic engineering from the Tokyo Institute of Technology, Tokyo, Japan, in 1995.

From 1995 to 2004, he joined the Japan Atomic Energy Research Institute as a Researcher and developed power supplies and superconducting coils for nuclear fusion reactors. Since 2004, he has been an Associate Professor of the Division of Electrical, Electronic and Information Engineering, Osaka University, Osaka, Japan. His areas of research involve applications of power electronics for power systems.



**Toshifumi Ise** (M'86) was born in 1957. He received the B.Eng., M.Eng., and Doctor of Engineering degrees in electrical engineering from Osaka University, Osaka, Japan, in 1980, 1982, and 1986, respectively.

From 1986 to 1990, he was with the Nara National College of Technology, Nara, Japan. Since 1990, he has been with the Faculty of Engineering, Osaka University, where he is currently a Professor of the Division of Electrical, Electronic and Information Engineering, Graduate School of Engineering. His research interests are in the areas of power electronics

and applied superconductivity for power systems including superconducting magnetic energy storage and future power systems including many distributed generations.